Direct numerical simulation of transitional pulsatile stenotic flow using Lattice Boltzmann Method

Kartik Jain[1, 2, a)]
[1)] *Simulation Techniques and Scientific Computing, University of Siegen, Hölderlinstr. 3, 57076 Siegen,* Germany
[2)] *Center for Biomedical Computing, Simula Research Laboratory, N-1325 Lysaker,* Norway

(Dated: 6 January 2016)

The present contribution reports direct numerical simulations of pulsatile flow through a 75% eccentric stenosis using the Lattice Boltzmann Method (LBM). The stenosis was previously studied by Varghese, Frankel, and Fischer [1] in a benchmark computation, and the goal of this work is to evaluate the LBM and the solver *Musubi* for transitional flows in anatomically realistic geometries. A part of the study compares the LBM simulation results against the benchmark and evaluates the efficacy of most basic LBM scheme for simulation of such flows. The novelty lies in the computation of Kolmogorov micro-scales by performing simulations that consist of up to $\sim 700 \times 10^6$ cells. Recommendations on the choice of spatial and temporal resolutions for simulation of transitional flows in complex geometries naturally arise from the results.

The LBM results show an excellent agreement with the previously published results thereby validating the method and the solver *Musubi* for the simulation of transitional flows. The study suggests that with a prudent calibration of the parameters, the LB method, due to its simplicity and compute efficiency has advantages for the simulation of such flows.

I. INTRODUCTION

Direct numerical simulation (DNS) is a way of numerically simulating flow in arbitrary geometries by resolving all the temporal and spatial scales that might appear in a transitional or a turbulent flow. Consequently this technique requires very high spatial and temporal resolutions and more compute power. Spectral methods and classical computational fluid dynamic (CFD) techniques like finite element method (FEM) and finite volume method (FVM) have been commonly employed for the simulation of flows. Spectral methods indeed are the most well established technique for the simulation of transitional *incompressible* flows as they allow for an increase in effective resolution with ease. In complex anatomical geometries however, which are the main goal of this and related work[2] are still difficult to be computed using spectral methods.

The Lattice Boltzmann Method (LBM) is an alternative technique for the simulation of low Mach number incompressible flows[3–6]. Although well established, due to its novelty the LBM results are sometimes met with skepticism, much of which is attributed to its *indirect* nature i.e. the method converges to the incompressible Navier-Stokes equations under the continuum limits of low Mach and Knudsen numbers[4,7] instead of a direct discretization of the Navier-Stokes equations. A question then materializes if DNS from such an indirect method is indeed direct. A comparison of LBM with spectral methods by Succi, Benzi, and Higuera [3] suggested excellent agreement between the two methods although not much work has been done in this direction after that. A reliable computation of transitional flow with LBM requires an effective tuning of the so called lattice parameters, as the errors in LBM that scale with the order of squared Mach number (Ma^2) can lead to unassuring results[8]. The excellent compute efficiency of the LBM algorithm however makes it a promising method for simulation of transitional flows in complex geometries at large scale

[a)] Electronic mail: kartik.jain@uni-siegen.de

PeerJ PrePrints | https://doi.org/10.7287/peerj.preprints.1548v3 | CC-BY 4.0 Open Access | rec: 6 Jan 2016, publ: 6 Jan 2016

with the advent of modern supercomputers.

The LBM solver *Musubi*[9–11] was specifically designed for high performance computing architectures to address large scale problems, and it scales on all the federal compute resources of GERMANY namely *Juqueen*, *SuperMUC* and the *Hazel Hen*. *Musubi* solver, even though is verified and validated thoroughly[9,10,12] for laminar and turbulent flows, a thorough validation has not been done for transitional and pulsating flows[1]. Swayed by the need for validation, and in support of its extensive use in ongoing research efforts for the simulation of transitional physiological flows[2,13], this work re-simulates the pulsatile flow through the eccentric stenosis that was previously studied in[1,14].

Since the emphasis is on the LBM, I will particularly focus on the role of parameters like the relaxation scheme of LBM, and space and time resolutions in *reproducing* results of previous DNS reported in[1]. To assess the quality of DNS, I will compute and quantify the Kolmogorov length and time scales, and will discuss the conditions under which going down to these scales might benefit the engineer while simulating physiological flows. The results show an excellent agreement with Varghese, Frankel, and Fischer[1] thereby increasing the confidence on the LBM and the solver *Musubi* for such applications. The Kolmogorov micro-scales and the recommendations that are provided in this work present a new *state of the art* as no computations, of the order of Kolmogorov micro-scales have been reported in literature to the author's knowledge. The results thus have the potential for retrospect in future, and for use as means for comparison.

II. METHODS

The eccentric stenosis geometry used for this study was similar to the models employed in the experiments of stenotic flow by[15,16]. The stenosis axis was offset by 0.05D, D being the vessel diameter, in the eccentric model. The eccentric stenosis geometry used for simulations is shown in figure 1(a). The offset of 0.05D from the axisymmetric counterpart (not studied here) is represented in figure 1(b), where the dashed line shows the eccentric case and black shows the axisymmetric. The presence of eccentricity here acts as a trigger to transitional flow. The pre and post-stenotic regions of the vessel were respectively extended by 3 and 18 vessel diameters as measured from the throat of stenosis.

The Womersley solution for laminar, pulsatile flow through rigid tubes was used as inlet boundary condition, which is specified as:

$$\left.\begin{aligned} \frac{u_x}{u_c} &= [1-r^2] + A\left[1 - \frac{J_0(i^{3/2}\alpha 2r/D)}{J_0(i^{3/2}\alpha)}\right] sin(\omega t),\\ \frac{u_y}{u_c} &= 0,\\ \frac{u_y}{u_c} &= 0 \end{aligned}\right\} \tag{1}$$

where u_c is the cycle-averaged centerline inlet velocity, A is the amplitude of pulsation, J_0 is the Bessel function of type 0, ω is the angular frequency of pulsation, and α is the non-dimensional Womersley parameter ($= \frac{1}{2}D\sqrt{\omega/\nu}$, where ν is the kinematic viscosity). The Womersley parameter defines the extent to which the laminar profile departs from quasi-steadiness, an effect that becomes significant when $\alpha = 3$.

The parameters and normalizations mentioned above are chosen to replicate the flow conditions of experiments of Ahmed and Giddens[16] and simulations of Varghese, Frankel, and Fischer[1]. The Reynolds number based on the main vessel diameter, D, and the mean inlet centerline velocity, u_c was 600 with minima and maxima of 200 and 1000. The value of A and α in equation 1 were 0.667 and 7.5 respectively. The velocity waveform at the inlet was sinusoidal and recordings were made in intervals of T/6 where T is the period of pulsation (depicted in figure 2).

---

[1] *Musubi*, along with other softwares within the APES framework is available as an open source tool for download under: https://bitbucket.org/apesteam/musubi

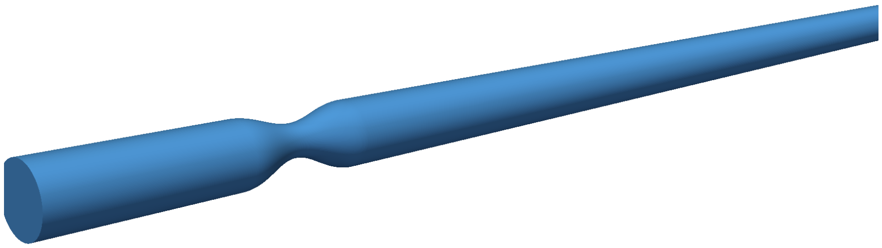

(a)stenosis geometry

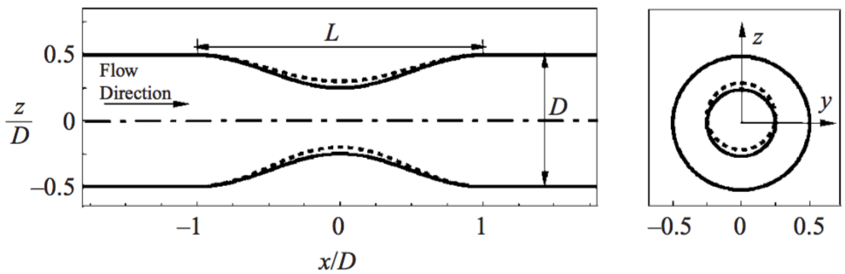

(b)offset from the symmetric stenosis that introduces eccentricity

FIG. 1: The eccentric geometry of stenosis used in the study. Lower part of the figure shows front and side views of the stenosis where solid line denotes the axisymmetric model and dashed line denotes the eccentric case. x is the streamwise direction and y and z are cross-stream directions.

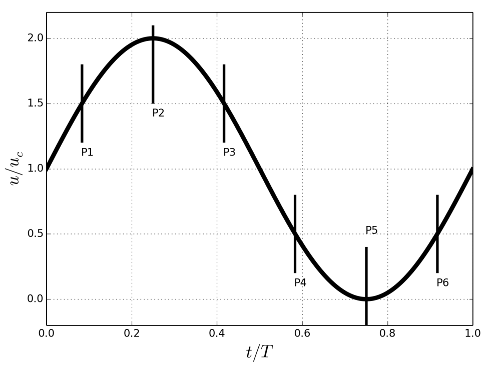

FIG. 2: Axial centerline velocity at the vessel inlet. The measurements were made at 6 time points in the sinusoidal cycle that are indicated in the plot.

Direct Numerical Simulations

The simulation tool chain is contained in the end-to-end parallel framework APES (adaptable poly engineering simulator)[11,17]. Meshes were created using the mesh generator *Seeder*[18]. I have used the single relaxation scheme Bhatnagar-Gross-Krook (BGK) out of the various LBM relaxation schemes implemented in *Musubi* as BGK is the simplest (and most efficient) relaxation scheme of the LBM algorithm. I performed two sets of simulations – one with moderate/low resolutions (LR) and one with extremely high resolutions (HR), down to the Kolmogorov microscales. The resulting parameters are listed in table I. The space and time have been non-dimensionalized for the simulation, and of interest here are the number of lattice cells along the diameter of the main channel and that along the throat

	δx	δt	#Cells diameter	#Cells throat	#Cells
LR	64	30×10^{-6}	156	40	$\sim 83 \times 10^6$
HR	32	7.5×10^{-6}	312	80	$\sim 680 \times 10^6$

TABLE I: The spatial and temporal discretization of eccentric stenosis. The space and time have been non-dimensionalized, and of relevance here is the number of cells along the diameter and stenotic throat.

of the stenosis. The time step is coupled with the grid spacing in LBM as $\delta t \sim \delta x^2$, which reflects the *diffusive time scaling* necessary to recover the incompressible Navier-Stokes equation from the Lattice Boltzmann Equation[4]. The BGK relaxation parameter was set to $\Omega = 1.94$ in the present study that keeps the lattice Mach number within the stability limits of the LBM[7,8]. The vessel walls were assumed to be rigid and a no-slip boundary condition, described by a bounce-back rule in LBM was prescribed. The implementation of this boundary condition ensures stability and provides reasonable accuracy. While other accurate implementations of no-slip wall approximation could have been employed[19], this particular boundary condition was chosen to maintain the principle intention of this study i.e. employment of *off the shelf* schemes of the LBM to assess its suitability in such simulations. The D3Q19 stencil of the LBM algorithm was employed which means 19 discrete velocity directions per fluid cell, or 19 degrees of freedom. Stencils with larger number of degrees of freedom can be employed but it has previously been suggested that the gain in accuracy for low Re flows is not appreciable compared to the cost of memory and computation[20]. At the outlets, zero pressure was prescribed which is described by a high-order extrapolation scheme within the LBM algorithm[21].

LR and HR computations were executed using 1000 and 9600 cores respectively of the *Hazel Hen* supercomputer installed at the High Performance Computing center in Stuttgart, Germany. The *Hazel Hen* contains a total of 185 088 cores of Intel(R) Xeon(R) CPU E5-2680 v3 (30M Cache, 2.50 GHz). *Hazel Hen* is one of the main federal compute resources in Germany and is ranked at number 8 in the current listing of top supercomputers[2]. A detailed account of the performance and scalability of *Musubi* can be found elsewhere[9,11]. Computation of each cycle required $\sim$ 36 minutes for LR simulations and $\sim$ 32 minutes for the HR simulations. The compute time mentioned here seems remarkably efficient, but is not comparable with Varghese, Frankel, and Fischer[1] as those computations were done in 2007 using a completely different architecture and CPUs, and a comparison of computational efficiency is not the intention of this study.

[2] http://top500.org

Flow analysis

The analysis of a turbulent or transitional flow follows the statistical principles as statistics, due to the chaotic behavior of the flow are the only reproducible quantities[22,23]. A total of $n = 22$ (where initial 2 cycles are discarded from analysis) cycles were computed from both LR and HR simulations and were ensemble averaged for analysis. The ensemble average over $\mathbf{n}$ cycles is defined as:

$$\overline{u}(x,t) = \frac{1}{n}\sum_{k=0}^{n-1} u(x, t+kT) \tag{2}$$

where $u(x,t)$ is the instantaneous point wise velocity field, $\mathbf{x}$ denotes the spatial coordinates, $\mathbf{t}$ is the time and $\mathbf{T}$ is the period of cycle. The instantaneous three-dimensional velocity field was decomposed into a mean and a fluctuating part using Reynolds' decomposition i.e.

$$u_i(x,t) = \bar{u}_i(x) + u'_i(x,t) \tag{3}$$

The Turbulent Kinetic Energy (TKE) is derived from the fluctuating components of the velocity in 3 directions as:

$$k = \frac{1}{2}\left(u_x'^2 + u_y'^2 + u_z'^2\right) \tag{4}$$

A power spectral density of the TKE, computed using Fourier transforms provides information about the frequency components present in the flow, and can be related to the Kolmogorov energy decay.

The Q-criterion

The Q-criterion was preferred in the present study for the visualization of coherent flow structures as it shares properties with both the vorticity and pressure criterion[24]. The Q-criterion is the second invariant of the velocity gradient tensor $\nabla\mathbf{u}$, and reads:

$$Q = \frac{1}{2}(\Omega_{ij}\Omega_{ij} - S_{ij}S_{ij}) \tag{5}$$

where

$$\Omega_{ij} = \frac{1}{2}\left(\frac{\partial u_i}{\partial x_j} - \frac{\partial u_j}{\partial x_i}\right) \quad (6)$$

and

$$S_{ij} = \frac{1}{2}\left(\frac{\partial u_i}{\partial x_j} + \frac{\partial u_j}{\partial x_i}\right) \quad (7)$$

are respectively the anti-symmetric and symmetric components of $\nabla \mathbf{u}$.

The Q-criterion can be physically viewed as the balance between the rotation rate $\Omega^2 = \Omega_{ij}\Omega_{ij}$ and the strain rate $S^2 = S_{ij}S_{ij}$. Positive Q isosurfaces confine the areas where the strength of rotation overcomes the strain - making those surfaces eligible as vortex envelopes. Several interpretations of Q-criterion have been proposed, see for example Robinson [25] which recasts Q in a form which relates to the vorticity modulus ω:

$$Q = \frac{1}{4}(\omega^2 - 2S_{ij}S_{ij}). \quad (8)$$

This implies that the Q is expected to remain positive in the core of the vortex as vorticity increases as the center of the vortex is approached.

DNS quality assessment with Kolmogorov microscales

The smallest structures that can exist in a turbulent flow are based on Kolmogorov's theory[22]. Viscosity dominates and the TKE is dissipated into heat at the Kolmogorov scale[22]. The Kolmogorov microscales are generally described in terms of the rate of dissipation due to the turbulent kinetic energy, which results in equations containing 4th order terms[22,23]. The Kolmogorov scales, for simplicity, can also be computed in terms of local friction velocity $u_* = \sqrt{\nu||s||}$ where s_{ij} is the *fluctuating* component of strain rate defined as:

$$s_{ij} = \frac{1}{2}\left(\frac{\partial u_i'}{\partial x_j} + \frac{\partial u_j'}{\partial x_i}\right) \quad (9)$$

and ν is the kinematic viscosity. As the physical quantities have been non-dimensionalized for the present study, the viscosity ν used for the computation of Kolmogorov micro-scales is the *lattice viscosity* that is formulated on the basis of BGK relaxation parameter Ω as:

$$\nu = \frac{1}{3}\left(\frac{1}{\Omega} - \frac{1}{2}\right) \quad (10)$$

The Kolmogorov length, time and velocity scales are then respectively estimated as:

$$\eta \equiv \nu/u_* \quad (11)$$

$$\tau_\eta \equiv \nu/u_*^2 \quad (12)$$

$$u_\eta \equiv u_* \quad (13)$$

Based on these scales, the quality of the spatial and temporal resolution of a simulation is estimated by computing the ratio of δx and δt against corresponding Kolmogorov scales i.e.

$$l^+ = \frac{u_*\delta x}{\nu}. \quad (14)$$

$$t^+ = \frac{u_*^2\delta t}{\nu}. \quad (15)$$

Ideally these ratios should be ~ 1 but in practice it has been observed that a l^+ of the order of $\mathcal{O}(10)$ is usually enough for the simulation of moderate Reynolds' numbers transitional flows[26].

III. RESULTS

Figure 3(a) and 3(b) depict the axial centerline velocities over the last $n = 6$ cycles obtained from LR and HR simulations respectively. Ensemble averaged counterparts for $n = 20$ cycles are shown in figure 4(a) and 4(b). Whereas the main flow captured by LR and HR simulations is similar, high resolutions seem to capture larger fluctuations particularly in post-stenotic regions (x=3-5D), and the differences between LR and HR are mostly visible in time periods when the flow starts to decelerate (time

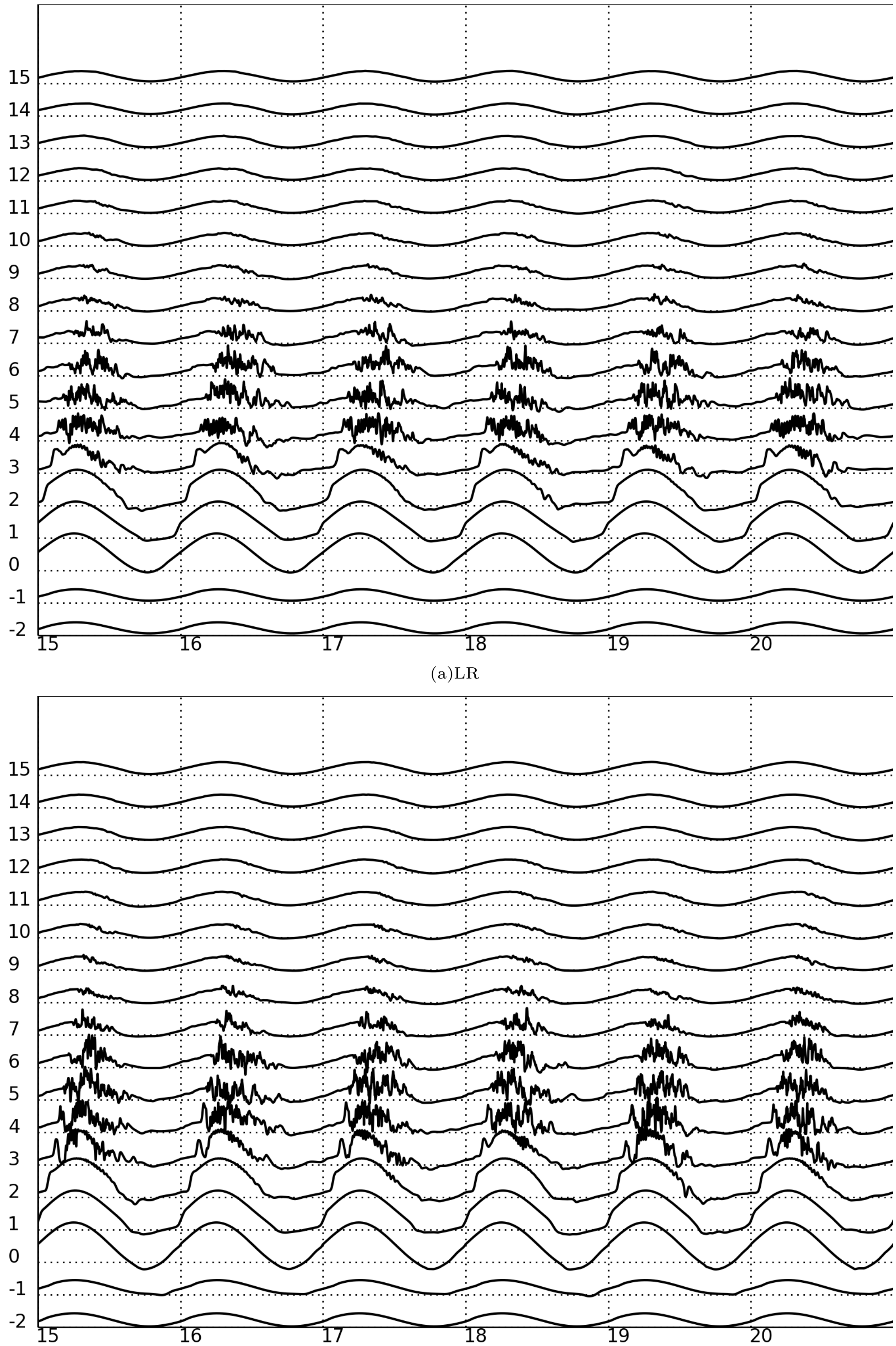

(a)LR

(b)HR

FIG. 3: Temporal evolution of the normalized centerline axial velocity, u/u_c over the last 6 cycles out of total 20 that were simulated, as a function of axial distance through stenosis, shown for LR and HR simulations.

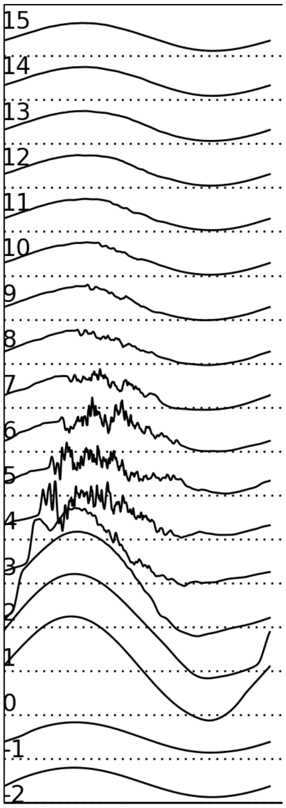

(a)LR

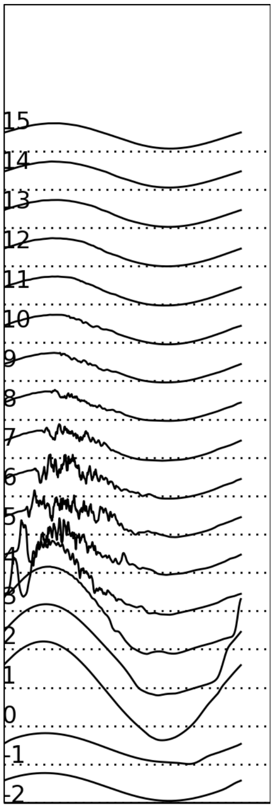

(b)HR

FIG. 4: Normalized centerline axial velocity ensemble averaged for $n = 20$ cycles shown for LR and HR simulations.

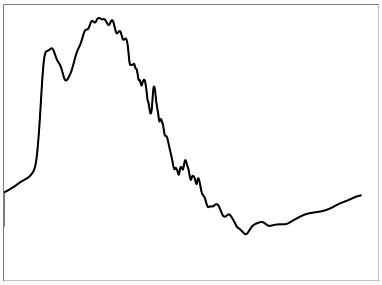

(a)P3

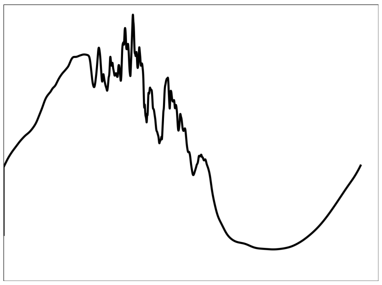

(b)P7

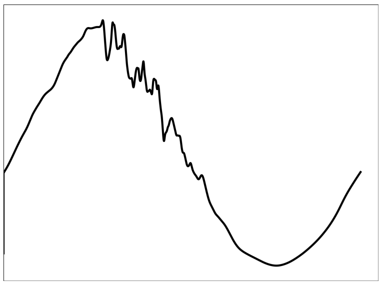

(c)P8

FIG. 5: Ensemble averages at axial centerline locations $x = 3, 7\&8D$ to magnify the fluctuations during deceleration and the re-laminarization of flow during acceleration.

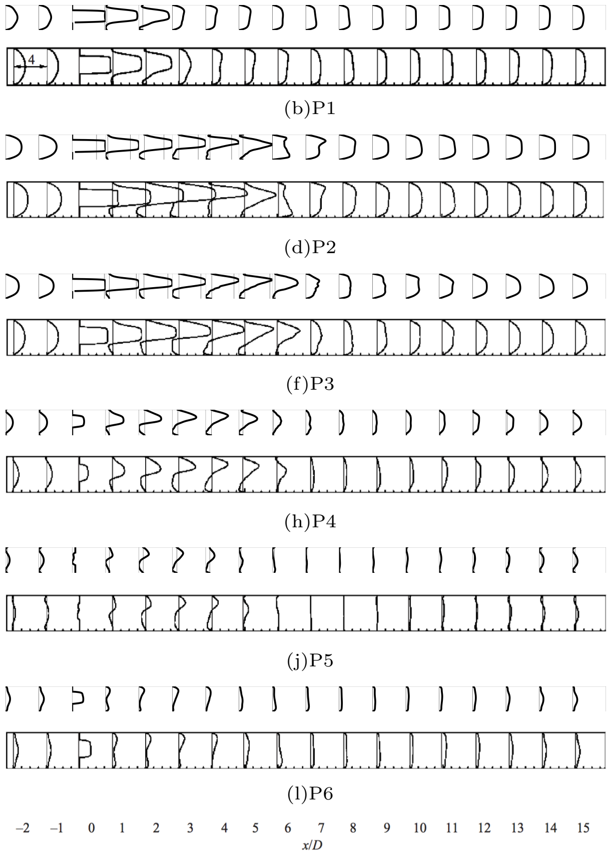

FIG. 6: Sequence of ensemble-averaged axial velocity profiles, $\langle u \rangle / u_c$ at observation points P1-P6 (top down) in the x-z plane. The top row of each point depicts computations from *Musubi* followed by the corresponding image from the benchmark computations from NEK5000.

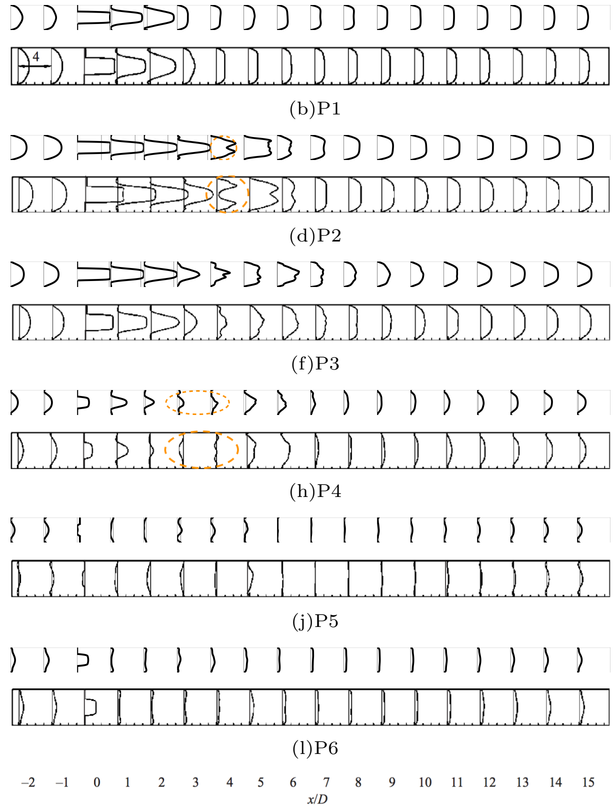

FIG. 7: Sequence of ensemble-averaged axial velocity profiles, $\langle u \rangle / u_c$ at observation points P1-P6 (top down) in the x-y plane. The top row of each point depicts computations from *Musubi* followed by the corresponding image from the benchmark computations from NEK5000.

instants P2 to P4). This observation would characterize LR setup as *converged*, though as would be seen in the turbulent characteristics, some intricate features might be suppressed by low resolutions.

The ensemble averaged quantities look largely similar for LR and HR simulations as the minute dynamics that were captured by HR are smeared out upon averaging. Subtle differences remain in the post-stenotic regions due to higher gradients in these regions. The remainder of the text would thus employ LR simulation results when ensemble averaged quantities are discussed and HR will be talked about only when instantaneous quantities are of interest.

Figure 5 shows the ensemble average at axial centerline locations $x = 3, 7$ & $8D$ from fig. 4(a) to highlight the loss of coherence patterns in the flow during deceleration phases, and the re-laminarization of the flow during acceleration. The stabilization of the flow in late-acceleration phases is location dependent, as the fluctuations seem to reduce beyond $x > 7D$. The regions between $x = 4D$ and $x = 6D$ represent highly chaotic behavior and larger cycle-to-cycle variations whereas the flow starts to become laminar in regions far-off from the stenosis throat.

Figure 6 and 7 respectively show the upstream velocity field in xz and xy axial bisecting planes. The velocity is ensemble averaged for n=20 cycles after

2 initial cycles that have been discarded from analysis. Corresponding plots from Varghese, Frankel, and Fischer [1] are also shown below each plot computed from *Musubi* for a direct visual comparison. An overall agreement is portrayed by this figure and the noticeable differences are highlighted under orange circles, and details are discussed in section IV.

Turbulent Characteristics of the Flow

Figure 8 shows the frequency spectra of the turbulent kinetic energy computed from centerline axial velocity at varying distance from the stenosis throat from LR simulations whereas figure 9 shows the same from HR simulations. The fluctuations are higher at locations x=3-6D and the flow starts to re-laminarize beyond x=9D – an observation that is consistent with the instantaneous and ensemble averaged velocity fields. The spectra at these locations indicate a large number of frequencies in the inertial subrange. The viscosity starts to dominate at frequencies of $\sim 10^4$ Hz up to x=7D. At locations $x > 10D$, flow can be considered largely laminar as the PSD is mostly below 10^{-10} for frequencies more than 10^3 Hz.

Comparison of the power spectrum plots from LR and HR simulations reveals a generic pattern whereby higher frequencies are detected by HR simulations due to small δt. The qualitative patterns are similar for both resolutions and as discussed later, the choice of resolutions is generally case dependent.

Vortex structures

Figure 10 and 11 show the ensemble averaged vorticity magnitude across the xz and xy planes respectively from LR simulations. The main patterns look similar to Varghese, Frankel, and Fischer [1], though LBM has detected some miniature vortices due to higher spatial and temporal magnitudes. It may be explicitly mentioned that the ensemble average for $n = 3$ cycles only is taken to educe the vortices, which would otherwise be smeared out if ensemble average over larger number of cycles are taken. When ensemble average for larger number of cycles is taken, the vortices are expected to die away and mimic Varghese, Frankel, and Fischer [1] more closely, as due to cycle-to-cycle variations, the location of vortices rapidly changes from one cycle to another. The eduction of instantaneous miniature vortices is in fact an important feature of DNS and is representative of the excellent control of numerical viscosity in LBM algorithm[3,13].

Figure 12 shows the vortex structures at 4 observation points during the 22nd cycle for LR simulations. The vortices are educed by the Q-criterion discussed in subsection II. The vortices begin to die during P5 and P6 due to re-laminarization of flow and are thus not shown in this figure. It is particularly interesting to observe that the majority of vortices lie along $x > 4D$ where the flow transits to main-stream turbulence, and was also reminiscent in the PSD plots. Some detached vortices are attached along the stenosis throat which is a consequence of higher strain along this region.

A mentionable aspect of this study is the *cycle-to-cycle* variations in the flow. As a result of transition to turbulence, the characteristics of flow vary from one cycle to another, and one cycle is not superimposable to another as would be expected, for example in a laminar flow. This aspect is highlighed in figure 13 which shows the centerline velocity at $x = 3D$ over 10 cycles as thin lines in the background. The black-line depicts the ensemble average over the 10 cycles and the dotted black lines represent standard deviation ($\pm\sigma$). It is immediately observed that all the lines overlap with each other during acceleration of the flow as a result of acceleration induced re-laminarization whereas there are large deviations when the flow transitions during deceleration phase, and it continues up to the complete deceleration before re-laminarizing by acceleration.

Kolmogorov microscales

Table II lists the l^+ and t^+ for LR and HR simulations. The ration are computed at the observation point P2 along x=4D during the 20th cycle as the fluctuation in strain rate was maximal at this location during P2, which implies maximum dissipation during the whole simulation. The employed resolu-

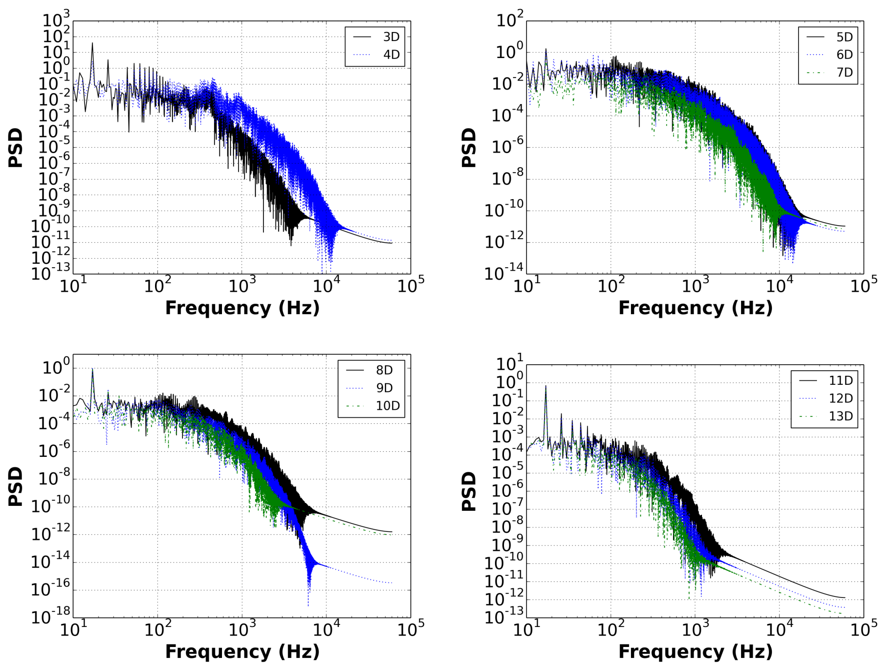

FIG. 8: Energy spectra of the turbulent kinetic energy computed at the centerline from LR simulations. The locations represent distance in diameters from the stenosis.

	δx	δt	l^+	t^+
LR	64	30×10^{-6}	2.67	0.84
HR	32	7.5×10^{-6}	1.10	0.53

TABLE II: The ratio of spatio-temporal scales (l^+, t^+) in the simulation and the Kolmogorov microscales for different resolutions.

tions are ample to resolve the rapidly varying structures expected in a turbulent flow[26]. Whereas the δx of LR is ~ 3 times of the Kolmogorov length scale, in a minor transitional flow in relatively less complex geometry like the presented stenosis, it should be enough for simulations as is also evident from the results.

IV. DISCUSSION

Analysis of the flow

Main things to observe (and to compare against Varghese, Frankel, and Fischer[1]) from the flow patterns of figure 6 and 7 were flow direction, peaks and nadirs as well as zones of flow reversal or recirculation. The flow field in the x-z plane exhibited satisfactory agreement with Varghese, Frankel, and Fischer[1]. The velocity was elevated at the throat of the stenosis, remained high in post-stenotic regions before becoming nearly constant near the end regions of the channel ($x > 11D$).

Similar agreement was seen for the x-y plane – though there were a few locations of disparity. For example, the post stenotic field at P2 (x=4) looked very different from Varghese, Frankel, and Fischer[1] (highlighted in orange circles). At P4, even the direction of flow disagreed at x=3 and x=4, which is

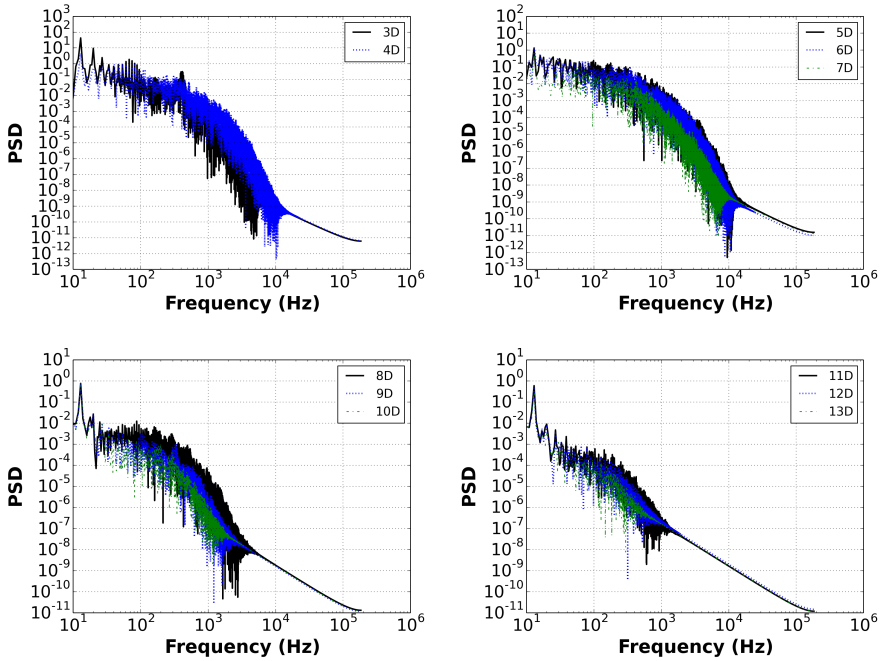

FIG. 9: Energy spectra of the turbulent kinetic energy computed at the centerline from HR simulations. The locations represent distance in diameters from the stenosis.

very surprising especially after an excellent agreement that was seen for x-z plane. The exact reason for this mismatch cannot be stated but it can be attributed to the different solution algorithms where minor differences are obvious. It should also be kept in mind that this comparison is one of *statistics* and involves round-off errors. Moreover, the perturbation that might be introduced as a result of wall roughness may stay in the flow up to an arbitrary number of cycles before being washed out completely. The boundary layer resolved by LBM and Spectral methods can be immensely different due to the distinct algorithms, and accuracy of one over the other can not be distinctly stated. The regions that are up-stream of stenosis, and in its vicinity have very high velocity gradients due to the onset of transition, and the wall boundary conditions are expected to influence the results dramatically. Whats most contenting is that in spite of different flow directions in these two locations, the flow field re-attained similarity beyond x=5 at all the time points, as did the flow field right at the stenosis throat.

Also, the flow fields from *Musubi* looked exactly the same as those from NEK5000 at P6 in the x-y plane, which portrays that the discrepancies seen during P4 and P5 might have been a result of the loss of coherence patterns caused by large decelerative forces, which were then overcame by the stabilization resulted by acceleration of flow. It is expected that if ensemble averaging over a larger number of cycles is done, these effects would wash away and the disparities would eventually vanish. That aspect however is not considered important due to the convincing agreement in other locations and time points, and would perhaps be useful when the simulation is actually re-conducted with NEK5000 as well.

Particularly interesting was the similarity in the flow patterns during P2 where the velocity of inflow is maximum, and P6 where the flow is in mid-acceleration phase after the deceleration. The pres-

PeerJ PrePrints | https://doi.org/10.7287/peerj.preprints.1548v3 | CC-BY 4.0 Open Access | rec: 6 Jan 2016, publ: 6 Jan 2016

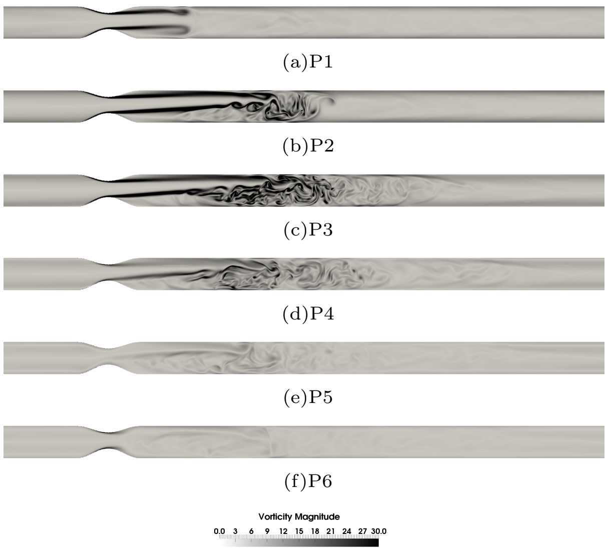

FIG. 10: Ensemble averaged vorticity magnitude, normalized by u_c/D at the x-z plane. Ensemble averaging is performed for ONLY $n = 3$ cycles to observe the intricate vortices which smear out when larger number of cycles are taken into account.

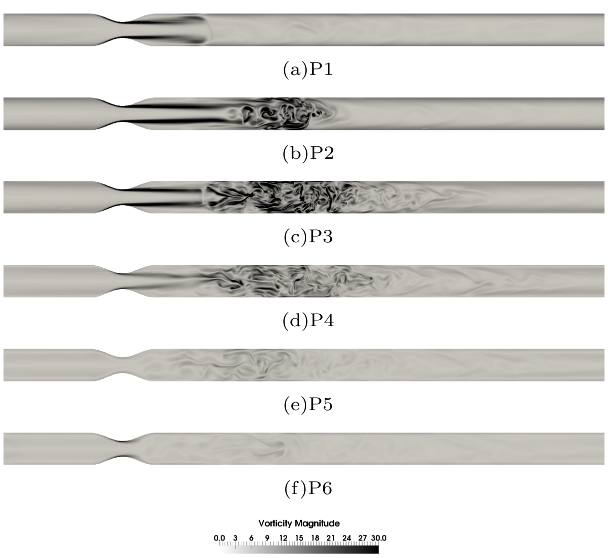

FIG. 11: Ensemble averaged vorticity magnitude, normalized by u_c/D at the x-y plane. Ensemble averaging is performed for ONLY $n = 3$ cycles to observe the intricate vortices which smear out when larger number of cycles are taken into account.

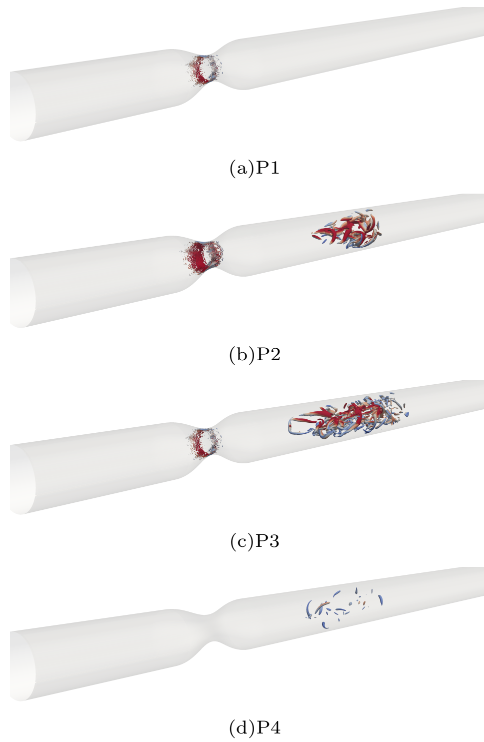

FIG. 12: Velocity colored Q-isosurfaces (Q=0.4) at the observation points P1-P4 during the 20th cycle for LR resolution. The velocity is normalized by u_c.

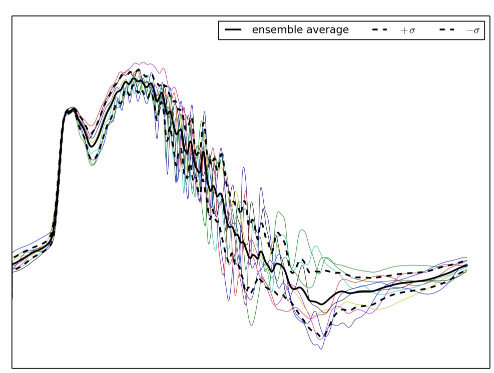

FIG. 13: The axial centerline velocity at $x = 3D$ for 10 different cycles overlapped over each other as thin lines. The black line represents the ensemble average over these 10 cycles whereas the standard deviation ($\pm\sigma$) is depicted by dotted lines.

ence of higher vortices during P3 than P2 as educed by the Q-Criterion (figure 12) appeared surprising at a first glance. From figure 2 one would expect highest vortices during P2 since it is the point with peak velocity. This is a consequence of the large decelerative forces that results in chaotic flow between P2 and P3 and creates distinct and larger vortex envelopes during P3. This was also observed in vorticity plots of figure 10 and figure 11.

The vorticity plots in figure 10 and 11 show some minute vortices in post stenotic areas even after ensemble averaging (though for only $n = 3$ cycles). The overall vorticity patterns are exactly similar to Varghese, Frankel, and Fischer [1]. It can easily be seen that if the sharpness of vortices is reduced upon ensemble averaging for more cycles, the patterns will look exactly similar as those in[1]. This prognosis is reminiscent of cycle-to-cycle variations that were clearly visible in instantaneous fields of figure 3. The initial conditions to any arbitrary cycle n are fed from the last state of previous cycle $n - 1$, which, in addition to the transitional nature of the flow itself makes flow field of each cycle look different. This is the reason why ensemble averaging is required for the analysis of transitional flows, and as discussed in[27], the computation of flow quantities poses additional challenges in such a flow.

Role of employed resolutions

As was seen from figures 3(a) and 3(b), the employment of high resolutions, that was directly at the order of Kolmogorov length and time scales (table II), did not provide much *improvement* to the simulated flow field except for the capture of some rapid spatial and temporal scales while educing larger cycle-to-cycle variations. The consumption of memory and compute time on the other hand became ~ 8 times with a higher resolution, though the computation was still remarkably fast. An unequivocal remark whether LR indeed is enough for simulating transitional flows in general, and transitional physiological flows in particular can not be made because physiological geometries are generally extremely complex. It has been shown in our studies of transitional aneurysmal flows that the solution indeed does change upon refinements when the geometry is not a regular conduit but a complex geometry[2,13]. Choice of resolutions in fact has been a subject of discussion with other numerical techniques as well, see for example research on this aspect about blood flow in aneurysms[28–30] as well as simulation of cerebrospinal fluid in the spinal canals[31].

In addition to that, the stenosis geometry studied here has one outflow which is perpendicular to the incoming flow. Presence of more outlets as well as the angle at which the downstream flow attacks these outlets is likely to upsurge the resolution requirements. Moreover, the stenosis may be viewed as a *controlled distortion* in a straight cylindrical pipe which is located at only one location in the pipe. In anatomically realistic geometries, arbitrary distortions can be present at multiple locations. The irregularity of such distortions can educe phenomena like *flow separation* and *hydraulic jumps* which would require employment of higher resolutions.

This study did not intend to establish the suitability of one numerical method over other as such a pursuit would require execution of different numerical codes on the same machine, and would require that the computer science methodologies like optimization techniques, compilation options etc. followed in implementation of the said codes are in agreement. One thing that enforces superiority of spectral methods is its ability to increase effective resolution[3] by increasing the polynomial order. Also Varghese, Frankel, and Fischer [1] employed higher mesh density near the walls and the stenosis throat unlike the even mesh employed by me in this study. Local grid refinement[9,10] is implemented and validated in *Musubi* framework and an accurate gauge on resolution/memory requirements can be accomplished only by exploring those techniques. What seems obvious at this point is that very low resolutions would suffice for an accurate simulation of hydrodynamics in the post stenotic regions beyond $x > 10D$, where the flow relaminarized and did not exhibit much spatial and temporal variations.

A mentionable aspect of this study in particular, and LBM simulated flows in general is the initial transients. I had to discard the initial 2 cycles from the analysis as they contain some spurious oscillations before converging to a physically meaningful outcome. Also, my specific focus on the relaminarization of flow during acceleration and the errors in LBM that scale of the order of Ma^2 would advocate the role of a proper tuning of the LBM parameters, which can lead to *specious* density fluctuations in the flow if not well-tuned[7,8], and are termed as compressibility errors. For these limitations of LBM, it has generally been considered unsuitable for steady problems and its inherently transient nature makes it a suited method for time dependent flows[7,32]. I shall not delve into details of the initial transients analysis of LBM and other methods, and a brief account for that can be found in[7,32].

It may be very well appreciated that the simplest off the shelf scheme of LBM reproduced an extremely complex flow with appreciable ease and efficiency. LB equations using multiple relaxation times (MRT) are intended to be more stable than the BGK as the additional relaxation times may be adjusted to suppress non-hydrodynamic modes that do not appear directly in the continuum equations, but may contribute to instabilities on the grid scale[33]. Such schemes would ostensibly be useful in more complex geometries as discussed above.

Outlook

The present work re-validates LBM and the *Musubi* solver particularly for transitional flows. The previous benchmark is extended for the LBM, Kolmogorov scales are quantified and recommendations on the choice of spatial and temporal resolutions in simulations have emerged from the study, which have implications particularly for the simulation of physiological flows of transitional nature in complex anatomical geometries.

The aspect of the onset of transition in this stenosis in particular has been an aspect of many recent studies[34,35]. The eccentricity in the present stenosis was introduced to trigger turbulent like flow as in a symmetric geometry and mesh, a perturbation is needed to cause the onset of turbulence[14]. The insights from this study can be used to explore the critical Reynolds number for transition in an axisymmetric stenosis and the influence of breaking of symmetry on critical Re can be identified with LBM, as was done by Samuelsson, Tammisola, and Juniper [34] using NEK5000.

Insight into fundamental physiological questions would be possible by incorporation of more physiologically realistic models like for example Non-Newtonian blood flow models and moving arterial walls. Whereas the Kolmogorov micro-scales are the smallest scales for turbulence in a flow – this hypothesis might not hold for blood[36] as the interaction of red blood cells (RBC) would obviate formation of eddies down to the Kolmogorov micro-scales. LBM models that are capable of modeling RBC interactions[37] should be evaluated in *Musubi* for better insight into such phenomena.

A final remark that can be made is that a LBM simulation on the same geometry with $\sim 8\times10^6$ cells was conducted using *Musubi* on my personal laptop, which completed one cycle in $\sim$ 26 hours. The fluctuations captured were less intense than the presented DNS, albeit the qualitatively agreement was very good. This suggests that with improving computer architectures, one might be able to simulate such problems on local computers with appreciable ease in future.

ACKNOWLEDGEMENTS

Thanks to *Prof. Kent-André Mardal* and *Prof. Sabine Roller* for supervision in my doctoral studies.

The study was suggested and motivated by *Dr. Bryn Martin* and *Mr. Soroush Heidari Pahlavian.* Soroush also helped me in creating the geometry and understanding the original benchmark.

I am specially thankful to the High Performance Computing Center, Stuttgart, GERMANY for compute resources on *Hazel Hen* and to the Leibniz Supercomputing Center, Munich, GERMANY for compute resources on the *SuperMUC*.

REFERENCES

[1] S. S. Varghese, S. H. Frankel, and P. F. Fischer, "Direct numerical simulation of stenotic flows. part 2. pulsatile flow," Journal of Fluid Mechanics **582**, 281–318 (2007).

[2] K. Jain and K.-A. Mardal, "Exploring the critical reynolds number for transition in intracranial aneurysms - highly

resolved simulations below kolmogorov scales," , 560 – 563 (2015), 2015 Computational and Mathematical Biomedical Engineering.

[3] S. Succi, R. Benzi, and F. Higuera, "The lattice boltzmann equation: a new tool for computational fluid-dynamics," Physica D: Nonlinear Phenomena **47**, 219–230 (1991).

[4] M. Junk, A. Klar, and L.-S. Luo, "Asymptotic analysis of the lattice boltzmann equation," Journal of Computational Physics **210**, 676–704 (2005).

[5] P. Lallemand and L.-S. Luo, "Theory of the lattice boltzmann method: Dispersion, dissipation, isotropy,galilean invariance, and stability," Physical Review E **61**, 6546 (2000).

[6] P. Lallemand and L.-S. Luo, "Theory of the lattice boltzmann method: Acoustic and thermal properties in two and three dimensions," Physical review E **68**, 036706 (2003).

[7] M. Rheinländer, "Analysis of lattice-boltzmann methods," (2007).

[8] J. Latt, *Hydrodynamic limit of lattice Boltzmann equations*, Ph.D. thesis, University of Geneva (2007).

[9] M. Hasert, K. Masilamani, S. Zimny, H. Klimach, J. Qi, J. Bernsdorf, and S. Roller, "Complex fluid simulations with the parallel tree-based lattice boltzmann solver musubi," Journal of Computational Science (2013).

[10] M. Hasert, *Multi-scale Lattice Boltzmann simulations on distributed octrees*, Ph.D. thesis, Aachen, Techn. Hochsch., Diss., 2013 (2014).

[11] H. Klimach, K. Jain, and S. Roller, "End-to-end parallel simulations with apes," in *Parallel Computing: Accelerating Computational Science and Engineering (CSE)*, Vol. 25 (2014) pp. 703–711.

[12] M. Johannink, K. Masilamani, A. Mhamdi, S. Roller, and W. Marquardt, "Predictive pressure drop models for membrane channels with non-woven and woven spacers," Desalination **376**, 41–54 (2015).

[13] K. Jain, S. Roller, and K.-A. Mardal, "Transitional flow in intracranial aneurysms–a space and time refinement study below the kolmogorov scales using lattice boltzmann method," Computers & Fluids (2015).

[14] S. S. Varghese, S. H. Frankel, and P. F. Fischer, "Direct numerical simulation of stenotic flows. part 1. steady flow," Journal of Fluid Mechanics **582**, 253–280 (2007).

[15] S. A. Ahmed and D. P. Giddens, "Velocity measurements in steady flow through axisymmetric stenoses at moderate reynolds numbers," Journal of biomechanics **16**, 505–516 (1983).

[16] S. A. Ahmed and D. P. Giddens, "Pulsatile poststenotic flow studies with laser doppler anemometry," Journal of biomechanics **17**, 695–705 (1984).

[17] S. Roller, J. Bernsdorf, H. Klimach, M. Hasert, D. Harlacher, M. Cakircali, S. Zimny, K. Masilamani, L. Didinger, and J. Zudrop, "An adaptable simulation framework based on a linearized octree," in *High Performance Computing on Vector Systems 2011* (2012) pp. 93–105.

[18] D. F. Harlacher, M. Hasert, H. Klimach, S. Zimny, and S. Roller, "Tree based voxelization of stl Data," in *High Performance Computing on Vector Systems 2011* (2012) pp. 81–92.

[19] M. Bouzidi, M. Firdaouss, and P. Lallemand, "Momentum transfer of a boltzmann-lattice fluid with boundaries," Physics of Fluids **13**, 3452 (2001).

[20] R. W. Nash, H. B. Carver, M. O. Bernabeu, J. Hetherington, D. Groen, T. Krüger, and P. V. Coveney, "Choice of boundary condition for lattice-boltzmann simulation of moderate-reynolds-number flow in complex domains," Physical Review E **89**, 023303 (2014).

[21] M. Junk and Z. Yang, "Asymptotic Analysis of Lattice Boltzmann Outflow Treatments." Communications in Computational Physics , 1–11 (2011).

[22] S. B. Pope, *Turbulent flows* (Cambridge university press, 2000).

[23] P. A. Durbin and B. P. Reif, *Statistical theory and modeling for turbulent flows* (John Wiley & Sons, 2011).

[24] J. C. Hunt, A. Wray, and P. Moin, "Eddies, streams, and convergence zones in turbulent flows," in *Studying Turbulence Using Numerical Simulation Databases, 2*, Vol. 1 (1988) pp. 193–208.

[25] S. K. Robinson, "The kinematics of turbulent boundary layer structure," NASA STI/Recon Technical Report N **91**, 26465 (1991).

[26] P. Moin and K. Mahesh, "Direct numerical simulation: a tool in turbulence research," Annual review of fluid mechanics **30**, 539–578 (1998).

[27] C. Poelma, P. N. Watton, and Y. Ventikos, "Transitional flow in aneurysms and the computation of haemodynamic parameters," Journal of The Royal Society Interface **12**, 20141394 (2015).

[28] K. Valen-Sendstad and D. Steinman, "Mind the gap: Impact of computational fluid dynamics solution strategy on prediction of intracranial aneurysm hemodynamics and rupture status indicators," American Journal of Neuroradiology (2013).

[29] Y. Ventikos, "Resolving the issue of resolution," American Journal of Neuroradiology **35**, 544–545 (2014).

[30] K. Valen-Sendstad, K.-A. Mardal, M. Mortensen, B. A. P. Reif, and H. P. Langtangen, "Direct numerical simulation of transitional flow in a patient–specific intracranial aneurysm," Journal of Biomechanics **44**, 2826–2832 (2011).

[31] A. Helgeland, K.-A. Mardal, V. Haughton, and B. Anders Pettersson Reif, "Numerical simulations of the pulsating flow of cerebrospinal fluid flow in the cervical spinal canal of a chiari patient," Journal of Biomechanics (2014).

[32] S. Geller, M. Krafczyk, J. Tölke, S. Turek, and J. Hron, "Benchmark computations based on lattice-boltzmann, finite element and finite volume methods for laminar flows," Computers & Fluids **35**, 888–897 (2006).

[33] P. J. Dellar, "Incompressible limits of lattice boltzmann equations using multiple relaxation times," Journal of Computational Physics **190**, 351–370 (2003).

[34] J. Samuelsson, O. Tammisola, and M. Juniper, "Breaking axi-symmetry in stenotic flow lowers the critical transition reynolds number," Physics of Fluids (1994-present) **27**, 104103 (2015).

[35] S. Sherwin and H. M. Blackburn, "Three-dimensional instabilities and transition of steady and pulsatile axisymmetric

stenotic flows," Journal of Fluid Mechanics **533**, 297–327 (2005).
[36]L. Antiga and D. A. Steinman, "Rethinking turbulence in blood," Biorheology **46**, 77–81 (2009).
[37]C. Sun and L. L. Munn, "Lattice-boltzmann simulation of blood flow in digitized vessel networks," Computers & Mathematics with Applications **55**, 1594–1600 (2008).